Article

Synchronized Oscillations in Double-Helix B-DNA Molecules with Mirror-Symmetric Codons

Enrique Maciá [1]

[1] Departamento de Física de Materiales, Facultad CC. Físicas, Universidad Complutense de Madrid, E-28040 Madrid, Spain; emaciaba@fis.ucm.es

Abstract: A fully analytical treatment of the base-pair and codon dynamics in double-stranded DNA molecules is introduced, by means of a realistic treatment which considers different mass values for G, A, T, and C nucleotides and takes into account the intrinsic three-dimensional, helicoidal geometry of DNA in terms of a Hamitonian in cylindrical coordinates. Within the framework of the Peyrard-Dauxois-Bishop model we consider the coupling between stretching and stacking radial oscillations as well as the twisting motion of each base pair around the helix axis. By comparing the linearized dynamical equations for the angular and radial variables when going from the bp local scale to the longer triplet codon scale, we report an underlying hierarchical symmetry. The existence of synchronized collective oscillations of the base-pairs and their related codon triplet units are disclosed from the study of their coupled dynamical equations. The possible biological role of these correlated, long-range oscillation effects in double standed DNA molecules containing mirror-symmetric codons of the form XXX, XX'X, X'XX', YXY, and XYX is discussed in terms of the dynamical equations solutions and their related dispersion relations.

Keywords: double-stranded DNA; DNA dynamical models; correlated oscillations in macromolecules; epigenetic changes

1. Introduction

The specific role of certain physical properties on the possible biological function of macromolecules of biological interest still remains as a fundamental open question spurring ongoing research in theoretical biophysics. For instance, the study of charge migration through DNA strands of different length has opened new avenues to understand damage recognition processes or protein binding mechanisms at work in nucleic acids, naturally leading to the design of nanoscale devices aimed at sensing genomic mutations within the emerging field of nanobiotechnology [1–3]. In physiological conditions DNA double helix exhibits a full-fledged three-dimensional (3D) geometry, so that every two consecutive Watson-Crick base pairs (bps) stand nearly parallel to each other and they are twisted by a certain angle around the helix axis ($\theta_0 \simeq 36^o$ in equilibrium conditions). Now, full-atomistic modular dynamics simulations indicate that double-stranded DNA (dsDNA) undergoes large-scale global oscillatory motions dominated by rise and twist oscillations of the bps planes as a whole, which dominate the range of molecular conformations generated by thermal agitation. Since, by all indications, charge transfer between consecutive bps proceeds through the π - π aromatic orbital overlap among the stacked bps, one reasonably expects that structural fluctuations modifying their mutual overlapping as a function of time will strongly affect charge carriers' transport through dsDNA molecules at physiological temperatures [4–8]. In this scenario, the relative orientation of neighboring bases is ever changing, and the motion of consecutive bps can either occur in a synchronized manner or incoherently.

In this work we will focus on coherent dynamics arising from the coupling between the radial oscillations of complementary bases within Watson-Crick bps and the twisting motion of each bp as a whole around the helical axis. In this way, attending to the local symmetry of the structural unit cell formed by three consecutive bps (the so-called *codon* in genomics), we disclose a number of remarkable symmetries of the dynamical motion equations, naturally leading to the emergence of synchronized helical waves and orchestrated collective, long-range oscillation modes propagating through the dsDNA molecule. This correlated motion is very important in certain biological processes, such as denaturation and transcription [9], and it is most relevant to any biological process which relies on shape recognition. To this end, we will exploit the Peyrard-Dauxois-Bishop (PDB) model [10,11], which explicitly takes into account the stacking interaction, mediated by the orbital overlapping between adjacent bps and hydrogen bond distortions along the helix [12,13].

The paper is organized as follows. In Section 2 we introduce the model Hamiltonian describing the lattice dynamics, which is expressed in cylindrical coordinates in order to explicitly take into account the 3D geometry of the double helix DNA molecule. Then, in Section 3 we derive the dynamical equations of motion corresponding to the angular and radial variables for both single bps and triplets containing three consecutive bps each (codon units) in polyX-polyX′, polyXX′-polyX′X, and polyXYX-polyX′Y′X′ dsDNA polymers, where X′ stands for the complementary Watson-Crick base of the base X. By comparing the mathematical structure of bp and codon motion equations we realize that they become identical to each other upon a suitable variable change in certain particular cases, involving dsDNA chains composed of mirror-symmetric codons of the form XXX, XX′X, X′XX′, YXY, and XYX. In doing so, we disclose a number of characteristic frequencies, related to the presence of collective oscillations corresponding to both synchronized helical waves, for which the intertwined angular and radial variables share the same frequency value, and orchestrated long-range waves given by a superposition of two harmonic oscillations with different frequencies for twist and radial motions. The helical waves' dispersion relations for the acoustic and optical branches are analytically derived in Section 4, and the obtained results are compared to some available experimental results. In Section 5 we solve the codon dynamical equations, reporting on the presence of certain resonance conditions closely related to the nucleotides' mass values distribution. In the light of these results, the role of possible epigenetic changes in the resulting dynamical behavior of dsDNA molecules is discussed. Finally, the main conclusions of this work are summarized in Section 6.

2. Dynamical DNA Model Hamiltonian

When describing the phonon dynamics in DNA one can disregard the inner degrees of freedom of the nucleotides, since we can separate the fast vibrational motions of atoms about their equilibrium positions from the slower motions of molecular groups. Thus, in the lattice model shown in Figure 1 each nucleotide (base + sugar + phosphate) is regarded as a point mass, helically arranged and mutually connected by means of elastic springs describing the sugar-phosphate backbone along a given strand, and the interstrand H-bonding between complementary bases [14–16]. We explicitly take into consideration the mass difference among the four nucleotides, namely, $m_G = 347.05$, $m_A = 331.06$, $m_T = 322.05$, $m_C = 307.05$ amu, where the subscripts stand for guanine (G), adenine (A), thymine (T), and cytosine (C). By inspecting these values we realize that the mass of each bp as a whole is essentially the same, i. e., $M \equiv m_G + m_C \cong m_A + m_T \cong 653.5 \pm 0.5$ amu. Analogously, the bps' reduced mass, $\mu_n \equiv m_n m_n' / M$, take on very similar values as well (see Table 1). Adopting the reference frame indicated in Figure 1 the position of the nth nucleobase on the right strand can be expressed as $x_n = r_n \cos\varphi_n$, $y_n = r_n \sin\varphi_n$, and $z_n = c\varphi_n$, where n labels the considered bp along the dsDNA, r_n and φ_n are usual cylindrical coordinates, and $c = h_0/\theta_0$ is the rise parameter, where $h_0 \simeq 0.34$ nm (B-DNA form) is the equilibrium distance between two successive bp planes along the Z axis, and θ_0 is the equilibrium relative angular separation between neighboring bps. Thus, we can express the Euclidean distance between adjacent bases along the right strand as:

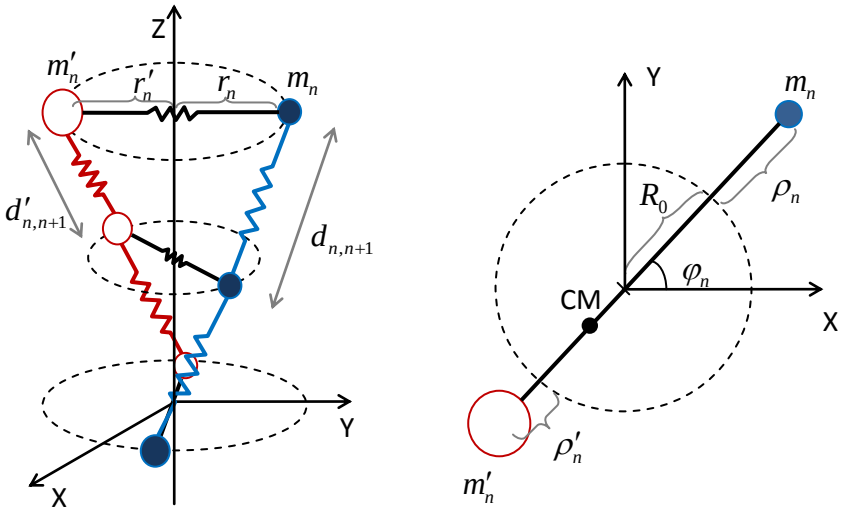

Figure 1. On the left, sketch of the dsDNA 3D lattice model showing the harmonic bonds between adjacent base pairs through the sugar-phosphate backbone and between complementary bases due to H-bonds . The right strand runs in the $5' \to 3'$ direction, wheras as the left strand runs in the antiparallel $3' \to 5'$ direction. On the right, detail of one of the bp planes, showing the effect the mass difference has on radial displacements, shifting the center of mass outside the axis of the helix. Reprinted from Physics Letters A, 376, Torrellas, G.; Maciá, E., Twist–radial normal mode analysis in double-stranded DNA chains, 3407–3410, Copyright (2012), with permission from Elsevier.

$$d_{n,n\pm1} = \sqrt{c^2\theta^2_{n,n\pm1} + (R_0+\rho_{n\pm1})^2 + (R_0+\rho_n)^2 - 2\,(R_0+\rho_{n\pm1})\,(R_0+\rho_n)\cos\theta_{n,n\pm1}} \tag{1}$$

($d'_{n,n\pm1}$ for the left strand is obtained by simply replacing $\rho_n \to \rho'_n$ in Eq.(1)), where we have defined $\theta_{n,n\pm1} = \pm\,(\varphi_{n\pm1} - \varphi_n)$ as the relative angle between two neighboring bps, and $\rho_n = r_n - R_0$ as the radial displacements about the equilibrium position ($R_0 = 1$ nm). In equilibrium, both distances reduce to the value $l_0 = d_{n,n\pm1}|_{eq.} = d'_{n,n\pm1}\Big|_{eq.} = \sqrt{h_0^2 + 4R_0^2\sin^2(\theta_0/2)} \simeq 0.685$ nm, where we have adopted $\theta_0 = \pi/5.2 \simeq 34.6^{\circ}$. We note that the distance between successive bps along the Z direction is proportional to the twist angle, thereby preserving the helical structure during the dynamical evolution [17]. It is further assumed that the dsDNA molecule does not move as a whole, so that the center of mass is constant for each bp, and the radial displacements about the equilibrium position satisfy $\rho'_n = \lambda_n\rho_n$, where $\lambda_n = m_n/m'_n$.

Accordingly, we can write the dsDNA molecule lattice Hamiltonian as [8,18]:

$$H_l = \frac{1}{2M}\sum_{n=1}^{N}\left(\frac{P^2_{\rho_n}}{\lambda_n} + \frac{P^2_{\varphi_n}}{\lambda_n\rho_n^2 + \xi^2 + 4R_0\rho_n m_n M^{-1}}\right) + U_B + U_{HS} \tag{2}$$

where n runs over the number N of bps, P_{ρ_n} and P_{φ_n} are the conjugate momenta of the nth bp radial and twist variables, respectively, and $\xi = \sqrt{c^2 + R_0^2} \simeq 1.147$ nm is related to the helical geometry of the system, so that $\xi\theta_{n,n\pm1}$ measures the helix arc length providing the shortest path between two points along a helical coil. In the limit of small radial and twist oscillations ($r_n \simeq R_0$, $\theta_{n,n+1} \ll 1$) Eq.(1) reads $d_{n,n\pm1} = \sqrt{R_0^2 + c^2}\;\theta_{n,n\pm1} \equiv \xi\theta_{n,n\pm1}$, so that the Euclidean distance coincides with the helix arc length in this case [19]. The potential term:

$$U_B = \frac{k_B}{2}\sum_{n=1}^{N-1}\left[(d_{n,n+1} - l_0)^2 + (d'_{n,n+1} - l_0)^2\right], \tag{3}$$

describes the harmonic interaction between neighboring bases along each backbone's strand, and the term:

$$U_{HS} = \sum_{n=1}^{N} D_n \left[e^{-\frac{\alpha_n}{2}(1+\lambda_n)\rho_n} - 1 \right]^2 + \frac{k_S}{8} \sum_{n=1}^{N-1} \left(1 + e^{-\frac{b}{2} u^+_{n+1,n}} \right) \left(u^-_{n+1,n} \right)^2, \tag{4}$$

describes the elastic energy related to radial displacements. The fist term in Eq.(4) represents the radial stretching of the hydrogen bonds connecting complementary bases in the opposite strands of the double helix by means of Morse potentials of depth D_n and width α_n [20]. The second term, with $u^{\pm}_{n,m} = (1+\lambda_n)\rho_n \pm (1+\lambda_m)\rho_m$, describes the stacking interaction between adjacent bps, whose role is to inhibit configurations with large relative radial displacements between neighboring pairs. This interaction gives rise to local constraints in nucleotide motions, and it is characterized by the exponential factor that effectively modulates an otherwise harmonic radial oscillation. This contribution is measured by the stacking stiffness k_S and the interaction range b parameters. The description of the radial degree of freedom via the non-linear potential given by Eq.(4) accounts for long-range cooperative elastic effects due to the distortion of hydrogen bonds and the overlap of the π-type orbitals [20], hence being more realistic than a purely harmonic approach. Indeed, this potential has proved successful in capturing denaturation as well as transcription initiation processes in several DNA model chains [21–23]. The model parameter values used in this work are listed in Table 1.

Table 1. Geometrical, dynamical, and potential model parameters adopted in the dsDNA model studied in this work. The same effective Morse potential is used to describe H-bonding in both GC and AT bps. The spring constant k_B is difficult to estimate, and different possible values, ranging from 0.04 to 0.5 eV Å^{-2} have been reported in the literature [24–29].

Geometrical	Dynamical	Potential
$\theta_0 = \pi/5.2$ rad	$M = 653.5$ amu	$b = 0.5$ Å^{-1} [15,30]
$h_0 = 0.34$ nm	$\lambda_{GC} = 1.130$	$\alpha = 5$ Å^{-1} [14,30,31]
$l_0 = 0.68$ nm	$\lambda_{AT} = 1.028$	$D = 0.15$ eV [21,30,31]
$R_0 = 1.00$ nm	$\mu_{GC} = 163.06$ amu	$k_S = 0.7$ eV Å^{-2} [21]
$\xi = 1.15$ nm	$\mu_{AT} = 163.15$ amu	$k_B = 0.04$ eV Å^{-2} [30]

3. Dynamical equations of motion

3.1. General expressions

From the lattice Hamiltonian given by Eq.(2) we can obtain the *linearized* canonical equations of motion [8]:

$$\ddot{\varphi}_n + \omega_\varphi^2 \left(2\varphi_n - \varphi_{n-1} - \varphi_{n+1} \right) = l_B^{-1} \omega_\varphi^2 [(1+\lambda_{n+1})\rho_{n+1} - (1+\lambda_{n-1})\rho_{n-1}], \tag{5}$$

and:

$$\ddot{\rho}_n + \omega^2_{\varphi SH,n}\rho_n - \frac{1}{2}(\omega^2_{\varphi S,n,n-1}\rho_{n-1} + \omega^2_{\varphi S,n,n+1}\rho_{n+1}) = \frac{a_B}{2}(1+\lambda_n^{-1})\omega_\varphi^2 \left(\varphi_{n-1} - \varphi_{n+1} \right), \tag{6}$$

where have introduced the characteristic lengths $l_B \equiv 2f_0/g_0$, with $f_0 = c^2\theta_0 + R_0^2 \sin\theta_0 \simeq 0.759$ nm^2, and $g_0 = R_0 \left(1 - \cos\theta_0\right) \simeq 0.177$ nm, so that $l_B \simeq 8.575$ nm (i. e., about 25 bps), and $a_B \equiv g_0\xi^2/f_0 \simeq 0.307$ nm, along with the twist frequency:

$$\omega_\varphi^2 \equiv \frac{2k_B}{M} \left(\frac{f_0}{\xi l_0} \right)^2, \tag{7}$$

and the coupled frequencies:

$$\omega^2_{\varphi SH,n} \equiv \Lambda_n(\omega^2_H + \omega^2_S + b^2_B\omega^2_\varphi) - 2b^2_B\omega^2_\varphi, \tag{8}$$

$$\omega^2_{\varphi S,n,n\pm1} \equiv (1+\lambda_{n\pm1})(1+\lambda_n^{-1})\omega^2_S - (\lambda_n^{-1}+\lambda_{n\pm1})b^2_B\omega^2_\varphi, \tag{9}$$

where $\Lambda_n \equiv \lambda_n^{-1}(1+\lambda_n)^2 = M/\mu_n$ is a dimensionless ratio, $\omega^2_H = D\alpha^2/(2M)$ is the radial stretch H-bonding frequency, $\omega^2_S = k_S/M$ is the lateral stacking oscillation frequency of bps, and $b_B \equiv a_B/\xi \simeq 0.268$ is a dimensionless factor. We note that Λ_n is invariant upon the transformation $\lambda_n \to \lambda_n^{-1}$, describing the permutation of nucleotides in the Watson-Crick bp (i.e., $m_n \leftrightarrow m'_n$). Making use of the M and μ_n values listed in Table 1 we get $\Lambda_{GC} = 4.008$ and $\Lambda_{AT} = 4.006$, so that we can safely make the approximation $\Lambda_n \simeq \Lambda = 4$, $\forall n$, and Eq.(8) can be reasonably approximated as $\omega^2_{\varphi SH} \simeq \Lambda(\omega^2_S + \omega^2_H) + 2b^2_B\omega^2_\varphi$, which no longer depends on the site label n.

The time scale of the bp twist Eq.(5) is completely determined by the characteristic frequency ω_φ, whereas the radial Eq.(6) involves three different characteristic frequencies, namely, ω_φ, $\omega_{\varphi S,n,n\pm1}$ (related to twist-stacking coupling), and $\omega_{\varphi SH}$ (fully coupling twist, stacking, and stretching interactions). The set of coupled Eqs.(5)-(6) describes the dynamics of general dsDNA molecules, where two kinds of bps can be arranged either periodically or aperiodically [32–36], and their mathematical structure clearly indicates the correlated nature of next-neighboring bps dynamics. It is then convenient to zoom out our perspective and consider the dynamics of consecutive triplets of bps, which are closely related to the so-called codon units in genomics. To this end, we properly add up the dynamical equations of consecutive bps corresponding to sites $n-1$, n, and $n+1$, grouping the resulting expression in terms of the collective variables $x_n \equiv 2\varphi_n - \varphi_{n-1} - \varphi_{n+1}$ and $y_n \equiv 2\rho_n - \rho_{n-1} - \rho_{n+1}$, to obtain:

$$\ddot{x}_n + \omega^2_\varphi\,(2x_n - x_{n-1} - x_{n+1}) = l_B^{-1}\omega^2_\varphi[(1+\lambda_{n+2})y_{n+1} - (1+\lambda_{n-2})y_{n-1} + H_x], \tag{10}$$

with:

$$H_x \equiv (\lambda_{n+2} - \lambda_{n-2})\rho_n + 2(\lambda_{n-2} - \lambda_{n-1})\rho_{n-1} + 2(\lambda_{n+1} - \lambda_{n+2})\rho_{n+1}, \tag{11}$$

and:

$$\ddot{y}_n + \omega^2_{\varphi SH}y_n - \frac{1}{2}(\omega^2_{\varphi S,n-1,n-2}y_{n-1} + \omega^2_{\varphi S,n+1,n+2}y_{n+1} - H_y) = \frac{a_B}{2}\omega^2_\varphi\left[(1+\lambda_{n-1}^{-1})x_{n-1} - (1+\lambda_{n+1}^{-1})x_{n+1} + 2G_y\right], \tag{12}$$

with:

$$H_y \equiv A_{n,n\pm1,n\pm2}\rho_n + 2B_{n,n-1,n-2}\rho_{n-1} + 2B_{n,n+1,n+2}\rho_{n+1}, \tag{13}$$

$$G_y \equiv (\lambda_{n+1}^{-1} - \lambda_n^{-1})\varphi_{n+1} + (\lambda_n^{-1} - \lambda_{n-1}^{-1})\varphi_{n-1} + (\lambda_{n-1}^{-1} - \lambda_{n+1}^{-1})\varphi_n, \tag{14}$$

where:

$$A_{n,n\pm1,n\pm2} = (2\lambda_n - \lambda_{n-2} - \lambda_{n+2})\Xi_{\varphi S} + \left[\lambda_{n+1}^{-1}(\lambda_n - \lambda_{n+2}) + \lambda_{n-1}^{-1}(\lambda_n - \lambda_{n-2})\right]\omega^2_S, \tag{15}$$

$$B_{n,n\pm1,n\pm2} = \left(\lambda_{n\pm2} - \lambda_{n\pm1} + \frac{\lambda_n - \lambda_{n\pm1}}{\lambda_n\lambda_{n\pm1}}\right)\Xi_{\varphi S} + \frac{\lambda_n\lambda_{n\pm2} - \lambda^2_{n\pm1}}{\lambda_n\lambda_{n\pm1}}\omega^2_S, \tag{16}$$

where $\Xi_{\varphi S} \equiv \omega^2_S - b^2_B\omega^2_\varphi$.

By comparing Eqs.(10) and (12), which describe the codon dynamics as a whole, with Eqs.(5) and (6), respectively describing the motion of their constituent bps, we can appreciate they exhibit a closely related algebraic structure, which is further highlighted when the auxiliary functions H_x, H_y, and G_y simultaneously vanish, so that Eqs.(10) and (12) become formally identical to Eqs.(5)-(6) upon the variable exchange $\varphi_n \leftrightarrow x_n$ and $\rho_n \leftrightarrow y_n$, respectively. In order to get $H_x = 0$ the bps mass ratios

λ_k must take on correlated values of the form $\lambda_{n-2} = \lambda_{n+2}$ and $\lambda_{n\pm2} = \lambda_{n\pm1}$. Such a relationship is naturally satisfied by bps sequences of the form 5′...XXYXX...3′, which display mirror symmetry with respect to the Y bp, located at the central nth site. On the other hand, the $G_y = 0$ and $H_y = 0$ conditions involve the central bp Y mass ratio value, leading to long-range correlations of the form $\lambda_n = \lambda_{n\pm1}$ (hence, $\lambda_{n-1} = \lambda_{n+1}$), and $\lambda_n = \lambda_{n\pm2}$, thereby requiring the presence of homogeneous bps sequences of the form 5′...XXXXX...3′.

3.2. Dynamics of homopolymer dsDNA chains

There exist four kinds of homopolymer dsDNA molecules, namely, polyG-polyC, polyA-polyT, polyT-polyA, and polyC-polyG chains, all of them satisfying $\lambda_k \equiv \lambda, \forall k$, so that $H_x = H_y = G_y = 0$ and Eqs.(5), (10), (6) and (12) respectively adopt the form:

$$\ddot{\varphi}_n + \omega_\varphi^2 \left(2\varphi_n - \varphi_{n-1} - \varphi_{n+1}\right) = A_\lambda \omega_\varphi^2 (\rho_{n+1} - \rho_{n-1}), \tag{17}$$

$$\ddot{x}_n + \omega_\varphi^2 \left(2x_n - x_{n-1} - x_{n+1}\right) = A_\lambda \omega_\varphi^2 (y_{n+1} - y_{n-1}), \tag{18}$$

and:

$$\ddot{\rho}_n + \omega_{\varphi SH}^2 \rho_n - \frac{\Omega_{\varphi S}^2}{2}(\rho_{n-1} + \rho_{n+1}) = B_\lambda \omega_\varphi^2 \left(\varphi_{n-1} - \varphi_{n+1}\right), \tag{19}$$

$$\ddot{y}_n + \omega_{\varphi SH}^2 y_n - \frac{\Omega_{\varphi S}^2}{2}(y_{n-1} + y_{n+1}) = B_\lambda \omega_\varphi^2 (x_{n-1} - x_{n+1}), \tag{20}$$

where $A_\lambda \equiv l_B^{-1}(1+\lambda)$ and $B_\lambda \equiv a_B(1+\lambda^{-1})/2$ are constants, and we have introduced the frequency $\Omega_{\varphi S}^2 \equiv \Lambda\omega_S^2 - (\lambda + \lambda^{-1}) b_B^2 \omega_\varphi^2 > 0$, since $b_B^2\omega_\varphi^2$ is about an order of magnitude smaller than ω_S^2 (see Table 2). We note that this characteristic frequency remains exactly the same upon the exchange $\lambda \to \lambda^{-1}$, describing a bp nucleotides' permutation. By inspecting Eqs.(17)-(20) we realize that the bps and codon dynamical equations of motion are *exactly* identical to each other upon the variable exchange $\varphi_n \leftrightarrow x_n$ and $\rho_n \leftrightarrow y_n$, respectively. This property can be regarded as expressing a *triplet renormalization operation* of the dynamical equations when going from the bp local scale to the longer triplet codon scale, hence disclosing an underlying scale-invariant hierarchical symmetry. In fact, by iterating the renormalization process grouping codons in successive triplets of nested codon units recurrently, we will obtain isostructural dynamical equations all the way long up to the entire DNA molecule itself, so that by solving this fundamental dynamical equations set we are actually capturing the main features of the dsDNA homopolymer dynamics as a whole.

Table 2. Characteristic frequencies and their related scale times in the lattice dynamics of polyX-polyX′, poly(XX′)-poly(X′X) and poly(XYX)-poly(X′Y′X′) dsDNA molecules with $\lambda = \lambda_{GC}$ and $\lambda^* = \lambda_{AT}$. The values for the alternative choice $\lambda = \lambda_{AT}$ and $\lambda^* = \lambda_{GC}$ slightly differ by just a few GHz. The frequencies $\omega_{\varphi H}$, $\Gamma_{\pm}$, Γ_{YXY}, and Γ_{XYX} are related to the orchestrated codon oscillations described in Section 5.

Oscillation	codon	ω_k	$(10^{12}$ rad s$^{-1})$	ν_k (THz)	τ_k (ps)
Twist		ω_φ	1.067	0.170	5.874
Stacking		ω_S	3.260	0.519	1.927
Stretching		ω_H	5.335	0.849	1.178
Twist-Stacking	X′XX′	${}^{-}\Omega_{\varphi S}$	6.122	0.974	1.026
	YXY	$\bar{\Omega}_{\varphi S}$	6.362	1.013	0.988
	XXX	$\Omega_{\varphi S}$	6.507	1.036	0.966
	XYX	$\tilde{\Omega}_{\varphi S}$	6.670	1.062	0.942
	XX′X	${}^{+}\Omega_{\varphi S}$	6.918	1.101	0.908
Twist-Stretching	XXX	$\omega_{\varphi H}$	10.685	1.701	0.588
Twist-Stacking-Stretching	XX′X	Γ_+	10.425	1.659	0.603
	XYX	Γ_{XYX}	10.498	1.671	0.599
	YXY	Γ_{YXY}	10.810	1.728	0.579
	X′XX′	Γ_-	10.911	1.737	0.576
		$\omega_{\varphi SH}$	12.511	1.991	0.502

3.3. Dynamics of poly(XX′)-poly(X′X) dsDNA molecules

Double-stranded DNA chains of the form poly(XX′)-poly(X′X) consist in a periodic repetition of a dinucleotide unit cell, and they provide the next step in an increasing chemical complexity route, going from the single-nucleotide based homopolymers considered in Section 3.2, to the fully informative aperiodically ordered DNA chains. Attending to the possible local ordering of the nucleotide sequence along the poly(XX′)-poly(X′X) chain, two kinds of codons can be identified, namely, X′XX′ and XX′X, both exhibiting a mirror symmetry leading to long-range correlations of the form $\lambda_{n-2} = \lambda_n = \lambda_{n+2} \equiv \lambda^{\pm 1}$ and $\lambda_{n-1} = \lambda_{n+1} \equiv \lambda^{\mp 1}$, $\forall n$, depending on whether the central nth site is occupied by a X or a X′ base, respectively. Therefore, $\omega^2_{\varphi S,n,n\pm 1} = \lambda^{-1}\omega^2_{\varphi S}$ and $\omega^2_{\varphi S,n\pm 1,n\pm 2} = \lambda\omega^2_{\varphi S}$, for X′XX′ codons, where $\omega^2_{\varphi S} \equiv \Lambda\omega^2_S - 2b^2_B\omega^2_\varphi > 0$. Accordingly, if we choose the reading frame so that the dsDNA sequence can be expressed as a periodic concatenation of codons of the form X′XX′, we have $H_x = 2(\lambda - \lambda^{-1})(\rho_{n-1} - \rho_{n+1})$, $H_y = 2(\lambda - \lambda^{-1})\omega^2_{\varphi S}(\rho_{n-1} + \rho_{n+1})$, and $G_y = (\lambda - \lambda^{-1})(\varphi_{n+1} - \varphi_{n-1})$, and Eqs.(5), (10), (6) and (12) are respectively written:

$$\ddot{\varphi}_n + \omega^2_\varphi\,(2\varphi_n - \varphi_{n-1} - \varphi_{n+1}) = \lambda^{-1}A_\lambda\omega^2_\varphi(\rho_{n+1} - \rho_{n-1}), \tag{21}$$

$$\ddot{x}_n + \omega^2_\varphi\,(2x_n - x_{n-1} - x_{n+1}) = A_\lambda\omega^2_\varphi\left[y_{n+1} - y_{n-1} + 2(1-\lambda^{-1})(\rho_{n-1} - \rho_{n+1})\right], \tag{22}$$

and

$$\ddot{\rho}_n + \omega^2_{\varphi SH}\rho_n - \frac{{}^{-}\Omega^2_{\varphi S}}{2}(\rho_{n-1} + \rho_{n+1}) = B_\lambda\omega^2_\varphi\,(\varphi_{n-1} - \varphi_{n+1}), \tag{23}$$

$$\ddot{y}_n + \omega^2_{\varphi SH}y_n - \frac{{}^{-}\Omega^2_{\varphi S}}{2}\left[\lambda^2(y_{n-1} + y_{n+1}) + 2(1-\lambda^2)(\rho_{n-1} + \rho_{n+1})\right] = B_\lambda\omega^2_\varphi\,[\lambda(x_{n-1} - x_{n+1}) + 2(1-\lambda)(\varphi_{n-1} - \varphi_{n+1})], \tag{24}$$

where ${}^{\pm}\Omega^2_{\varphi S} \equiv \lambda^{\pm 1}\omega^2_{\varphi S}$.

Completely analogous expressions are obtained if we choose the reading frame so that the dsDNA sequence can be expressed as a periodic concatenation of codons of the the form XX′X, by simply replacing $\lambda^{\pm 1} \to \lambda^{\mp 1}$ in the above expressions. As we see, Eqs.(21)-(22) and (23)-(24) do not exactly coincide with each other upon the renormalization transformation $\varphi_n \leftrightarrow x_n$ and

$\rho_n \leftrightarrow y_n$, except in the case $\lambda = 1$ (i.e., $m_n = m'_n$), which describes *mismatched* repeats of the form poly(XX')-poly(XX') or poly(X'X)-poly(X'X), that no longer contain complementary Watson-Crick bps. Therefore, at variance with the remarkable self-similar symmetry displayed by homopolymers, such as 5'- ...GGGGG...3' or 5' ...CCCCC...3', dsDNA chains based on an alternating sequence of both bases, such as 5'- ...GCGCGCGCGC...3', completely lack that symmetry property.

3.4. Dynamics of poly(XYX)-poly(X'Y'X') dsDNA molecules

Another instance of a dsDNA system exhibiting a suitable local mirror symmetry is provided by periodic DNA chains whose unit cell includes codons of the form XYX, so that the local bps arrangement around Y type bases reads 5'...XXYXX...3'. If we label the bps in such a way that the Y base occupies the n reference site, then we have the relationships $\lambda_{n\pm2} = \lambda_{n\pm1} \equiv \lambda$, and $\lambda_n \equiv \lambda^*, \forall n$, so that we get $H_x = 0$. Therefore, the bps and codon dynamical equations corresponding to the twist variables just coincide with Eqs.(17)-(18) previously obtained for the homopolymer case. On the other hand, we have:

$$H_y = 2\frac{\lambda^* - \lambda}{\lambda\lambda^*}\left[\lambda^*\Omega_+^2\rho_n + \lambda\Omega_-^2(\rho_{n-1} + \rho_{n+1})\right], \qquad G_y = \frac{\lambda^* - \lambda}{\lambda\lambda^*}(\varphi_{n+1} - \varphi_{n-1}), \tag{25}$$

where $\Omega_\pm^2 \equiv \lambda^{\pm1}\Xi_{\varphi S} + \omega_S^2$. Thus, the radial motion equations read:

$$\ddot{\rho}_n + \omega_{\varphi SH}^2\rho_n - \frac{\tilde{\Omega}_{\varphi S}^2}{2}(\rho_{n-1} + \rho_{n+1}) = B_{\lambda^*}\omega_\varphi^2(\varphi_{n-1} - \varphi_{n+1}), \tag{26}$$

where $\tilde{\Omega}_{\varphi S}^2 \equiv \Lambda^*\omega_S^2 - (\lambda + 1/\lambda^*)b_B^2\omega_\varphi^2$, with $\Lambda^* \equiv (1+\lambda)(1+\lambda^*)/\lambda^* \simeq 4.20$, and:

$$\ddot{y}_n + \omega_{\varphi SH}^2 y_n - \frac{\Omega_{\varphi S}^2}{2}(y_{n-1} + y_{n+1}) + \frac{\lambda^* - \lambda}{\lambda\lambda^*}\left[\lambda^*\Omega_+^2\rho_n + \lambda\Omega_-^2(\rho_{n-1} + \rho_{n+1})\right] =$$

$$B_\lambda\omega_\varphi^2\left[x_{n-1} - x_{n+1} + 2\frac{\lambda^* - \lambda}{\lambda^*(1+\lambda)}(\varphi_{n+1} - \varphi_{n-1})\right]. \tag{27}$$

Completely analogous expressions are obtained for poly(YXY)-poly(Y'X'Y') polymers by simply permuting $\lambda^* \leftrightarrow \lambda$ in Eqs.(25)-(27). By comparing Eqs.(26)-(27) two main differences can be drawn. Firstly, the frequencies $\Omega_{\varphi S}$ and $\tilde{\Omega}_{\varphi S}$ are different in general, and only coincide in the homopolymer case. Secondly, in the codon motion equations the bps variables explicitly appear in the factor $\lambda^* - \lambda$ terms, hence they do not coincide with each other upon the transformation $\rho_n \leftrightarrow y_n$.

Making use of the model parameters listed in Table 1 we obtain the values listed in Table 2 for the characteristic frequencies we have introduced through Sections 3.2-3.4, along with their related time scales. From the data listed in Table 2 we see that the time scale of pure angular motions, determined by the twist frequency, amounts to $\sim$ 6 ps, which are an order of magnitude slower than those corresponding to the fully coupled twist-stacking-stretching frequency $\omega_{\varphi SH}$. The time scale related to twist-stacking oscillations is close to 1 ps, while that related to twist-stretching motions range in within the 0.6 - 0.5 ps interval. For the sake of comparison, the transition times reported for intrastrand hole transfer in ds-GT$_n$GGG oligonucleotides, range from $\tau = 0.5$ ps for $n = 1$ to $\tau = 315$ ps for $n = 4$ [37]. Quite interestingly, the electrical response of biological dsDNA chains to light irradiation has been recently investigated in order to engineer a DNA-based molecular switch. In these experiments it was observed that electrical current turns on when the frequency of the incident light is above the 2 THz threshold [38], a figure very close to that listed for $\nu_{\varphi SH}$ in Table 2, a frequency involving energy enough to activate all the fundamental interactions present in the system Hamiltonian in a coupled way.

4. Helical waves related dispersion relations

Motivated by previous results [19,39], we look for solutions of the form $\varphi_n = \varphi_0 e^{i(\omega t - nq\xi)}$ and $\rho_n = \rho_0 e^{i(\omega t - nq\xi)}$, describing a helical wave propagating throughout the dsDNA with frequency ω and wave vector q, where $\varphi_0 \simeq 8^o = 0.14$ rad, and $\rho_0 \simeq 0.05$ nm, are the twist and radial oscillation amplitudes at ambient temperature, respectively [40]. In so doing, Eqs.(17) and (19) for dsDNA homopolymers can be expressed in the matrix form [8]:

$$\begin{pmatrix} G(q) - \omega^2 & 2iA_\lambda \omega_\varphi^2 \sin(q\xi) \\ -2iB_\lambda \omega_\varphi^2 \sin(q\xi) & H(q) - \omega^2 \end{pmatrix} \begin{pmatrix} \varphi_0 \\ \rho_0 \end{pmatrix} = \begin{pmatrix} 0 \\ 0 \end{pmatrix}, \tag{28}$$

where $G(q) \equiv 4\omega_\varphi^2 \sin^2(q\xi/2)$ and $H(q) \equiv \omega_{\varphi SH}^2 - \Omega_{\varphi S}^2 \cos(q\xi)$. The solution to Eq.(28) requires the matrix determinant to identically vanish, thereby leading to a biquadratic equation whose solutions yield the dispersion relations for the acoustic and optical phonon branches given by:

$$\omega_\pm^2(q) = \frac{1}{2}(H+G) \pm \frac{1}{2}\sqrt{(H-G)^2 + \Lambda^2 b_B^2 \omega_\varphi^4 \sin^2(q\xi)}. \tag{29}$$

Since $\Lambda b_B^2 \omega_\varphi^2$ is much smaller than both $\Lambda\omega_S^2$ and $\Lambda\omega_H^2$ terms, the exact dispersion relations given by Eq.(29) can be very well approximated by the simpler expressions:

$$\nu_-^2 = 4\nu_\varphi^2 \sin^2\left(\frac{q\xi}{2}\right) \qquad \nu_+^2 = \Lambda\left[\nu_H^2 + 2\nu_S^2 \sin^2\left(\frac{q\xi}{2}\right)\right], \tag{30}$$

in agreement with previously reported results [15,21].

By comparing Eqs.(17) and (21), along with Eqs.(19) and (23) we realize that Eq.(28) also holds for poly(XX')-poly(X'X) chains by simply replacing $A_\lambda \to \lambda^{\mp 1} A_\lambda$ and $\Omega_{\varphi S}^2 \to \lambda^{\mp 1}\omega_{\varphi S}^2$, respectively. Thus, we obtain the following dispersion relations for poly(XX')-poly(X'X) and poly(X'X)-poly(XX'), respectively:

$$\nu_-^2 = 4\nu_\varphi^2 \sin^2\left(\frac{q\xi}{2}\right) \qquad \nu_+^2 = \Lambda\left[\nu_H^2 + (1 - \lambda^{\mp 1}\cos(q\xi))\nu_S^2\right]. \tag{31}$$

Analogously, by comparing Eqs.(19) and (26) we realize that Eq.(28) holds for poly(XYX)-poly(X'Y'X') chains as well by simply replacing $B_\lambda \to B_{\lambda^*}$ and $\Omega_{\varphi S}^2 \to \tilde{\Omega}_{\varphi S}^2$, respectively, so that we get the following dispersion relations:

$$\nu_-^2 = 4\nu_\varphi^2 \sin^2\left(\frac{q\xi}{2}\right) \qquad \nu_+^2 = \Lambda\left[\nu_H^2 + (1 - a_{\lambda\lambda^*}\cos(q\xi))\nu_S^2\right], \tag{32}$$

where

$$a_{\lambda\lambda^*} \equiv \frac{\lambda(1+\lambda^*)}{\lambda^*(1+\lambda)}, \tag{33}$$

satisfies the relationship $a_{\lambda^*\lambda} = a_{\lambda\lambda^*}^{-1}$, and it takes on two possible values: $a_{GC,AT} = 1.0466$ and $a_{AT,GC} = 0.9555$.

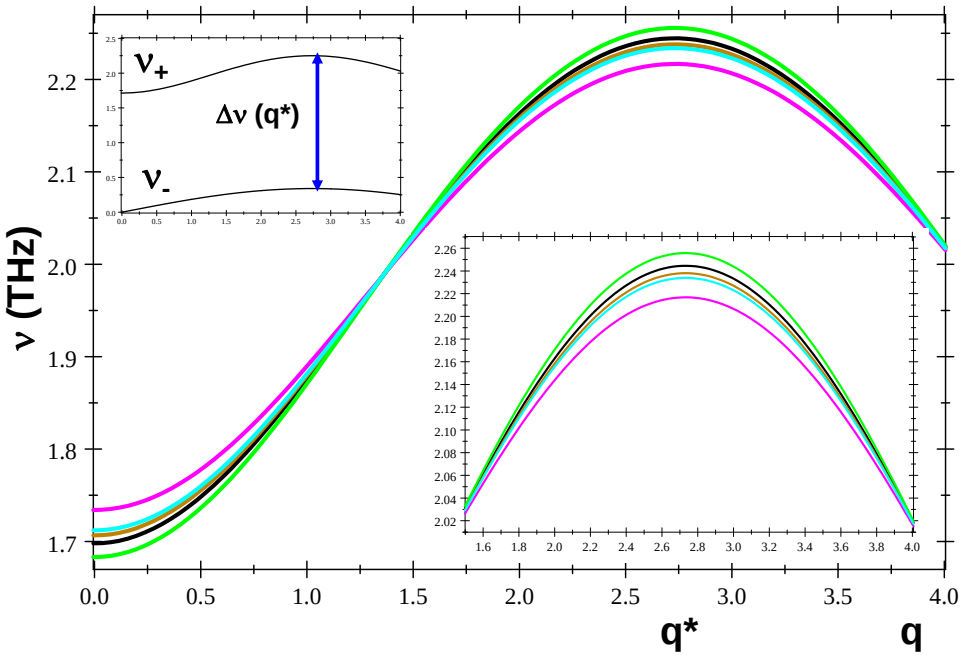

Figure 2. (Main frame) Optical phonon branches for polyG-polyC (black), poly(GC)-poly(CG) (magenta), poly(AT)-poly(TA) (siena), poly(GAG)-poly(CTC) (green), and poly(AGA)-poly(TCT) (light blue) dsDNA polymers, where q is measured in nm^{-1}, and we have used the values of the the model parameters and characteristic frequencies listed in Tables 1 and 2, respectively. (Low inset) Close up view of the optical branch curves shown in the main frame in the interval $1.5 \leq q \leq 4$. (Top inset) Acoustic $\nu_-(q)$ and optical $\nu_+(q)$ phonon branches for polyG-polyC dsDNA homopolymers. (Reprinted from Maciá, E. Base-Pairs' Correlated Oscillation Effects on the Charge Transfer in Double-Helix B-DNA Molecules. Materials 2020, 13, 5119).

By comparing Eqs.(30)-(32) we see that the acoustic branch of polyX-polyX', poly(XX')-poly(X'X) and poly(XYX)-poly(X'Y'X') chains is exactly the same, and it is completely determined by twist oscillations, so that it is insensitive to the particular nucleotide sequence order along the dsDNA chain. On the contrary, the optical branches depend on both stretch and stacking oscillations and they reflect the role of the underlying bps ordering throughout the chain, which is expressed by the presence of $\lambda^{\mp 1}$ and $a_{\lambda\lambda'}$ factors in Eqs.(31) and (32) for poly(XX')-poly(X'X) and poly(XYX)-poly(X'Y'X') chains, respectively. For homopolymer chains the $q = 0$ bandgap, $\Delta\nu_0 \equiv \nu_+(0) - \nu_-(0) = \sqrt{\Lambda}\nu_H \simeq 1.698$ THz ($\simeq 7$ meV), is fixed by the H-bond stretching frequency value, whereas it depends on both stacking and stretching frequencies for more complex dsDNA chains, according to the expressions $\Delta\nu_0 = 2\sqrt{\nu_H^2 + (1-\lambda^{-1})\nu_S^2}$ and $\Delta\nu_0 = 2\sqrt{\nu_H^2 + (1-a_{\lambda\lambda'})\nu_S^2}$ for poly(XX')-poly(X'X) and poly(XYX)-poly(X'Y'X') molecules, respectively. Therefore, the $q = 0$ bandgap of poly(XX')-poly(X'X) molecules is always somewhat wider than that of homopolymers, whereas in the case of poly(XYX)-poly(X'Y'X') polymers it can be wider or narrower depending on the nature of the Y bp. Indeed, by inspecting Figure 2 we observe that poly(GAG)-poly(CTC) chains exhibit the smaller $q = 0$ bandgap value (1.687 THz), while the wider bandgap (1.734 THz) corresponds to poly(GC)-poly(CG) chains. The maximum bandgap width occurs for $q^* = \pi/\xi \simeq 2.732$ nm^{-1}, as can be seen in the top inset of Figure 2, with $\Delta\nu(q^*) = 2\sqrt{\nu_H^2 + 2\nu_S^2} - 2\nu_\varphi \simeq 1.905$ THz for homopolymers. A close look at the bottom inset reveals that the wider the $q = 0$ bandgap the narrower the maximum bandgap at q^* for the considered dsDNA chains.

5. Orchestrated codon oscillations

In addition to the synchronized helical waves, for which the intertwined angular and radial variables share the same ω value, we can also disclose long-range correlated motions of the angular and radial variables in time, orchestrated in such a way that they simultaneoulsy satisfy the conditions $\varphi_{n-1}(t) = \varphi_{n+1}(t)$ and $\rho_{n-1}(t) = \rho_{n+1}(t)\ \forall n$. In that case, the collective variables read $x_n = 2(\varphi_n - \varphi_{n\pm1}) = \mp 2\theta_{n,n\pm1}$ and $y_n = 2(\rho_n - \rho_{n\pm1}) = \mp 2p_{n,n\pm1}$, where the collective motion variable $p_{n,n\pm1}$ plays for radial oscillations a role completely analogous to that played by the variable $\theta_{n,n\pm1}$ for twist ones. In terms of the revamped collective variables the codon dynamical Eqs.(10) and (12) can be respectively rewritten in the form:

$$\ddot{\theta}_{n,n\pm1} + 4\omega_\varphi^2 \theta_{n,n\pm1} = l_B^{-1}\omega_\varphi^2 \left[(\lambda_{n+2} - \lambda_{n+2}) p_{n,n\pm1} \mp \frac{H_x}{2} \right], \tag{34}$$

and:

$$\ddot{p}_{n,n\pm1} + \left[\omega_{\varphi SH}^2 - \frac{1}{2}(\omega_{\varphi S,n-1,n-2}^2 + \omega_{\varphi S,n+1,n+2}^2) \right] p_{n,n\pm1} \pm \frac{H_y}{4} = a_B \omega_\varphi^2 (\lambda_{n-1}^{-1} - \lambda_{n+1}^{-1}) \theta_{n,n\pm1}. \tag{35}$$

The condition $\rho_{n-1}(t) = \rho_{n+1}(t)$ guarantees that $H_x = 0$ for polyXX'-polyX'X dsDNA molecules (see Section 3.2). In addition, polyX-polyX' and poly XYX-poly X'Y'X' polymers satisfy the relationships $\lambda_{n-1} = \lambda_{n+1}$ and $\lambda_{n-2} = \lambda_{n+2}$ in a natural way. Accordingly, codon Eqs.(34)-(35) can be properly simplified to read:

$$\ddot{\theta}_{n,n\pm1} + 4\omega_\varphi^2 \theta_{n,n\pm1} = 0, \qquad \ddot{p}_{n,n\pm1} + \Gamma_u^2 p_{n,n\pm1} \pm \frac{H_y}{4} = 0, \tag{36}$$

where $\Gamma_u^2 \equiv \omega_{\varphi SH}^2 - \omega_{\varphi S,n\pm1,n\pm2}^2$ (u labels the DNA unit cell type), so that its precise value depends on the nature of the codons present in the considered dsDNA molecule. Thus, for polyX-polyX' polymers $\Gamma_X^2 \equiv \omega_{\varphi SH}^2 - \Omega_{\varphi S}^2 = \Lambda(\omega_H^2 + b_B^2\omega_\varphi^2) \equiv \omega_{\varphi H}^2$. This frequency accounts for the collective radial oscillations of XXX (alternatively, X'X'X') codons, describing a long-range oscillation where stacking interactions become ineffective, giving rise to a coupled twist-stretching mode which cannot be observed at the bp scale. Since homopolymers satisfy the $H_y = 0$ condition, the resulting dynamical equations of motion (36) become effectively decoupled in terms of simple harmonic motions with two different natural frequencies, namely, $2\omega_\varphi$ for twist, and $\omega_{\varphi H}$ for radial motions, respectively. Solving the twist harmonic expression $\theta_{n,n\pm1}(t) = \theta_0 \cos(2\omega_\varphi t + \delta_0)$ for the time variable, and plugging it into the radial harmonic expression $p_{n,n\pm1}(t) = p_0 \cos(\omega_{\varphi H} t + \delta_0')$, where the phases δ_0 and δ_0' are determined from the initial conditions, we get the relationship:

$$p_{n,n\pm1} = p_0 \cos\left[\frac{\omega_{\varphi H}}{2\omega_\varphi} \cos^{-1}\left(\frac{\theta_{n,n\pm1}}{\theta_0} - \delta_0 \right) + \delta_0' \right], \tag{37}$$

describing the spatial pattern of the long-range correlated motion in terms of the collective variables $\theta_{n,n\pm1}$ and $p_{n,n\pm1}$.

Making use of Eq.(13)-(16) into Eq.(36) we obtain the following expressions for the radial codon equations corresponding to polyXX'-polyXX', and polyXYX-polyX'Y'X' chains, respectively:

$$\ddot{p}_{n,n\pm1} + \Gamma_\pm^2 p_{n,n\pm1} = \pm(\lambda^{\pm1} - \lambda^{\mp1})\omega_{\varphi S}^2 \rho_n = \mp(\Gamma_+^2 - \Gamma_-^2)\rho_n, \tag{38}$$

where $\Gamma_\pm^2 = \omega_{\varphi SH}^2 - \lambda^{\pm1}\omega_{\varphi S}^2$, hence $\Gamma_+^2 - \Gamma_-^2 = (\lambda^{-1} - \lambda)\omega_{\varphi S}^2$, and:

$$\ddot{p}_{n,n\pm1} + \Gamma_{XYX}^2 p_{n,n\pm1} = \mp \frac{\lambda^* - \lambda}{2\lambda^*\lambda}(\lambda^* \Omega_+^2 + 2\lambda\Omega_-^2)\rho_n, \tag{39}$$

where:

$$\Gamma_{XYX}^2 \equiv \omega_{\varphi H}^2 + 2\frac{\lambda^* - \lambda}{\lambda^* \lambda}\left[(1+\lambda)\omega_S^2 - b_B^2\omega_\varphi^2\right]. \tag{40}$$

Completely analogous expressions are obtained for poly(YXY)-poly(Y'X'Y') polymers by simply permuting $\lambda^* \leftrightarrow \lambda$ in Eqs.(38)-(40). The obtained dynamical equations indicate that for the resonance conditions $\Gamma_+ = \Gamma_-$, for polyXX'-polyXX' chains, and $\lambda'\Omega_+^2 = -2\lambda\Omega_-^2$ for polyXYX-polyX'Y'X' chains, the twist and radial equations decouple from each other leading to two harmonic motions in a way completely analogous to that previously described for the homopolymers case. In the polyXX'-polyX'X case, the relationship given by Eq.(37) holds by simply replacing $\omega_{\varphi H} \to \Gamma_\pm$. It is important to note that this resonance can only take place for dsDNA molecules satisfying the mismatch condition $\lambda = 1$, so that it may be regarded as signaling the presence of local alterations in the due bp sequencing. Alternatively, within the framework of epigenetic processes, one may consider the attachment of a small molecule with the required mass value (i. e., $\Delta m = m_n - m_n'$) to the lighter pyrimidine nucleotide in order to get the required resonance condition $\lambda = 1$. In the polyXYX-polyX'Y'X' case the resonance condition leads to the expression:

$$\frac{\lambda\lambda^* + 2}{(1+\lambda)(2+\lambda^*)} = \left(\frac{\omega_S}{b_B\omega_\varphi}\right)^2 = \frac{k_S}{2k_B}\left(\frac{l_0}{g_0}\right)^2, \tag{41}$$

which depends on the mass ratio values λ and λ^*, along with the twist and stacking characteristic frequencies which, in turn, can be expressed in terms of model parameters.

The general solution to the dynamical equations for polyXX'-polyX'X polymers can be obtained from the knowledge of the general solution to the homogeneous version of Eq.(38) given by $\pi_n = A_0\cos(\Gamma_\pm t + \delta_0)$, plus the particular solution ansatz $\rho_n = -p_{n,n\pm1}$, leading to the diffential equation $\ddot{p}_{n,n\pm1} + \Gamma_\mp^2 p_{n,n\pm1} = 0$, whose solution reads $\tilde{\pi}_n = B_0\cos(\Gamma_\mp t + \delta_0')$. For the sake of simplicity we adopt the initial conditions $\dot{\rho}_n(0) = \dot{\rho}_{n\pm1}(0) = 0$, and $\rho_n(0) = -p_{n,n\pm1}(0)$, so that we get:

$$p_{n,n\pm1} = \pi_n + \tilde{\pi}_n = \pm 4\rho_0 \sin\left(\frac{|\,\Gamma_\pm - \Gamma_\mp}{2}t\right)\sin\left(\frac{\Gamma_\pm + \Gamma_\mp}{2}t\right) \equiv \pm 4\rho_0\sin(\gamma_- t)\sin(\gamma_+ t) = -\rho_n(t), \tag{42}$$

describing a modulated oscillation where $\gamma_- = 39$ GHz and $\gamma_+ = 1.698$ THz. Since $\rho_{n,n\pm1} = \rho_n \pm p_{n,n\pm1} = 2\rho_n$ we see that all the bps in the codon move in phase. A similar solution describing a modulated oscillation in opposite phase is obtained by choosing $\rho_n = p_{n,n\pm1}$ as the particular solution to the inhomogeneous differential Eq.(38). In this case, we get a larger high frequency value $\gamma_+ = 1.774$ THz. By following a completely analogous procedure Eq.(39) for polyXYX-polyX'Y'X' polymers can be solved in a similar way.

6. Conclusions

We have performed a systematic analytical study of the nucleotides' dynamics in dsDNA chains characterized by the presence of mirror-symmetric codons. By considering the mathematical structure of the dynamical equations at the local, single bp scale, and the triplet codon longer scale, two kinds of long-range, collective motions of nucleotides have been indentified on the basis of the symmetry properties of these equations upon the variable exchange $\varphi_n \leftrightarrow x_n$ and $\rho_n \leftrightarrow y_n$ describing a renormalization transformation involving suitable collective variables. For one thing, we have helical waves, characterized by intertwined angular and radial oscillations sharing the same frequency value. On the other hand, we have orchestrated motions of codon triplets where twist and radial variables harmonically vibrate with different values of their natural frequencies, giving rise to the presence of a modulated oscillation extending over the whole dsDNA molecule. We also have identified the possible existence of certain resonance conditions related to the presence of mismatch mutations involving a relatively small number of neighboring nucleotides. Indeed, a remarkable feature of our treatment is that, as far as we are concerned on the DNA dynamical bahavior, the chemical nature of bps plays no

role at all, since the nucleotide sequence along the dsDNA molecule is fully described in terms of the bps mass ratio parameters λ_k. As a consequence, the behavior of the reported correlated oscillations can be significantly perturbed when the DNA molecule is bonded with other small molecules, or it is subjected to epigenetic processes such as methylation (the addition of a methyl group (-CH_3) to one of the bases), which modify the nucleobase effective mass, hence changing the mass ratio parameter λ among nucleotides. Generally speaking the presence of ligands attached onto the sugar-phosphate backbone affects the mass distribution in a local region of the DNA molecule. This effect can be properly accounted for in terms of a change in the values of parameters λ_k and M, thereby modifying the related characteristic frequencies values. Thus, any effective bp mass increase leads to a slow down of frequencies ω_φ, ω_H, and ω_S, along with their related coupled frequencies. In addition, the reduction of the twist frequency value makes the acoustic dispersion relation slope to decline, so that the sound speed is reduced as well, ultimately leading to a lower thermal conductivity around the place where the small molecule has been bonded. Furthermore, a smaller ω_φ value will wide the gap between the acoustic and optical branches (see Figure 2).

Funding: This research received no external funding.

Acknowledgments: I sincerely thank Prof. Constantinos Simserides for his continued interest in my research works and Prof. Evgeni B. Starikov for illuminating conversations on physico-chemical aspects of DNA molecules. I gratefully thank Ms. Victoria Hernández for a critical reading of the manuscript.

Conflicts of Interest: The authors declare no conflict of interest.

Abbreviations

The following abbreviations are used in this manuscript:

dsDNA	double-stranded DNA
bp	base pair
A	adenine
C	cytosine
G	guanine
T	thymine
PDB	Peyrard-Dauxois-Bishop

References

1. Chakarborty, T. Editor. *Charge Migration in DNA: Perspectives from Physics, Chemistry and Biology*. Springer, Berlin, 2007.
2. Treadway, C.; Hill, M. G.; Barton, J. K. Charge transport through a molecular pi-stack: double helical DNA *Chem. Phys.* **2002**, *281*, 409–428.
3. Zwang, T.J.; Tse, E. C. M.; Barton, J.K. Sensing DNA through DNA Charge Transport *ACS Chemical Biology* **2018**, *13*, 1799-1809; DOI: 10.1021/acschembio.8b00347.
4. Starikov, E. B.; Fujita, T.; Wanatabe, H.; Sengoku, Y.; Tanaka, S.; Wenzel, W. Effects of molecular motion on charge transfer/transport through DNA duplexes with and without base pair mismatch *Molecular simulation* **2006**, *32*, 759–764.
5. Berlin, Y. A.; Grozema, F. C.; Siebbeles, L. D. A.; Ratner, M. A. Charge transfer in donor-bridge-acceptor systems: Static disorder, dynamic fluctuations, and complex kinetics *J. Phys. Chem. C* **2008**, *112*, 10988–11000.
6. Starikov, E. B.; Quintilla, A.; Nganou, C.; Lee, K. H.; Cuniberti, G.; Wenzel, W. Single-molecule DNA conductance in water solutions: Role of DNA low-frequency dynamics *Chem. Phys. Lett.* **2009**, *467*, 369–374.
7. Bruinsma, R.; Grüner, G.; D'Orsogna, M. R.; Rudnick, J. Fluctuation-facilitated charge migration along DNA *Phys. Rev. Lett.* **2000**, *85*, 4393–4396.
8. Maciá, E. Base-Pairs' correlated oscillation effects on the charge transfer in double-helix B-DNA molecules. *Materials* **2020**, *13*, 5119.
9. Peyrard, M. Nonlinear dynamics and statistical physics of DNA *Nonlinearity* **2004**, *17*, R1-R40.
10. Peyrard, M.; Bishop, A. R. Statistical mechanics of a nonlinear model for DNA denaturation *Phys. Rev. Lett.* **1989**, *62*, 2755–2758.

11. Dauxois, T.; Peyrard, M. Entropy-driven transition in a one-dimensional system *Phys. Rev. E* **1995**, *51*, 4027–4040.
12. Peyrard, M.; Cuesta-López,S.; Angelov, D. Experimental and theoretical studies of sequence effects on the fluctuation and melting of short DNA molecule *J. Physics.: Condensed Matter* **2009**, *21* , 034103.
13. Shinwari, W.; Deen, M. J.; Starikov, E. B.; Cuniberti, G. Electrical Conductance in Biological Molecules *Adv. Funct. Mater.* **2010**, *20*, 1865–1883.
14. Barbi, M.; Cocco, S.; Peyrard, M. Helicoidal model for DNA opening *Phys. Lett. A* **1999**, *253*, 358–369.
15. Cocco, S.; Monasson, R. Statistical mechanics of torque induced denaturation of DNA *Phys Rev. Lett.* **1999**, *83*, 5178–5181.
16. Agarwal J.; D. Hennig, D. Breather solutions of a nonlinear DNA model including a longitudinal degree of freedom *Physica A* **2003**, *323*, 519–533.
17. Krisch, M.; Mermet, A.; Grimm, H.; Forsyth, V. T.; Rupprecht, A. Phonon dispersion of oriented DNA by inelastic x-ray scattering *Phys. Rev. E* **2006**, *73*, 061909.
18. Torrellas, G.; Maciá, E. Twist–radial normal mode analysis in double-stranded DNA chains *Phys. Lett. A* **2012**, *376*, 3407–3410.
19. Maciá, E. Electrical conductance in duplex DNA: Helical effects and low-frequency vibrational coupling *Phys. Rev. B* **2007**, *76*, 245123.
20. Dauxois, T.; Peyrard, M.; Bishop, A. R. Entropy-driven DNA denaturation *Phys. Rev. E* **1993**, *47*, R44-R47.
21. Cocco, S.; Monasson, R. Theoretical study of collective modes in DNA at ambient temperature *J. Chem. Phys.* **2000**, *112*, 10017–10033.
22. Campa, A.; Giansanti, A. Experimental tests of the Peyrard-Bishop model applied to the melting of very short DNA chains *Phys. Rev. E* **1998**, *58*, 3585–3588.
23. Cule, D.; Hwa, T. Denaturation of Heterogeneous DNA *Phys. Rev. Lett.* **1997**, *79*, 2375–2378.
24. Lee, O.; Jeon, J. H.; Sung, W. How double-stranded DNA breathing enhances its flexibility and instability on short length scales *Phys. Rev. E* **2010**, *81*, 021906.
25. Michoel, T.; Van de Peer, Y. Helicoidal transfer matrix model for inhomogeneous DNA melting *Phys. Rev. E* **2006**, *73*, 011908.
26. Okonogi, T. M.; Alley, S. C.; Harwood, E. A.; Hopkins, P. B.; B. H. Robinson, B. H. Phosphate backbone neutralization increases duplex DNA flexibility *Proc. Natl. Acad. Sci. U. S. A. 2002*, *99*, 4156–4160.
27. Duduială, C. I.; Wattis, J. A. D.; Dryden, I. L.; Laughton, C. A. Nonlinear breathing modes at a defect site in DNA *Phys. Rev. E* **2009**, *80*, 061906.
28. S. Zdravković, M. V. Satarić, Single-molecule unzippering experiments on DNA and Peyrard-Bishop-Dauxois model *Phys. Rev. E* **2006**, *73*, 021905.
29. Ghorbani, M.; Rafiee, F. M. Geometrical correlations in the nucleosomal DNA conformation and the role of the covalent bonds rigidity *Nucleic Acids Res.* **2011**, *39*, 1220–1230.
30. Barbi, M.; Lepri, S.; Peyrard, M.; Theodorakopoulos, N. Thermal denaturation of a helicoidal DNA model *Phys. Rev. E* **2003**, *68*, 061909.
31. Leal, M. R.; Weber, G. Sharp DNA denaturation in a helicoidal mesoscopic model *Chem. Phys. Lett.* **2020**, *755*,137781.
32. E. Maciá-Barber, *Aperiodic Structures in Condensed Matter: Fundamentals and Applications*; Taylor and Francis, CRC Press: Boca Raton, FL, USA, 2009; pp. 209–297.
33. Maciá, E. Charge transfer in DNA: effective Hamiltonian approaches *Z. Kristallogr.* **2009**, *224*, 91–95.
34. Mantela, M.; Lambropoulos, K.; Theodorakou, M.; Simserides, C. Quasi-Periodic and Fractal Polymers: Energy Structure and Carrier Transfer *Materials* **2019**, *12*, 2177.
35. Lambropoulos, K.; Simserides, C. Periodic, quasiperiodic, fractal, Kolakoski, and random binary polymers: Energy structure and carrier transport *Phys. Rev. E* **2019**, *99*, 032415.
36. Lambropoulos, K.; Simserides, C. Tight-binding modeling of nucleic acid sequences: Interplay between various types of order or disorder and charge transport *Symmetry* **2019**, *11*, 968.
37. Landi, A.; Borrelli, R.; Capobianco, A.; Peluso, A. Transient and enduring electronic resonances drive coherent long distance charge transport in molecular wires *J. Phys. Chem. Lett.* **2019**, *10*, 1845–1851.
38. Behnia, S.; Fathizadeh, S.; Javanshour, E.; Nemati, F. Light-driven modulation of electrical current through DNA sequences: Engineering of a molecular optical switch *J. Phys. Chem.B* **2020**, *124*, 3261–3270.

39. Maciá, E. $\pi - \pi$ orbital resonance in twisting douplex DNA: Dynamical phyllotaxis and electronic structure effects *Phys. Rev. B* **2009**, *80*, 125102.
40. Young, M. A.; Ravishanker, G.; Beveridge, D. L. A 5-nanosecond molecular dynamics trajectory for B-DNA: analysis of structure, motions, and solvation *Biophys. J.* **1997**, *73*, 2313–2336.